Journal Homepage: -www.journalijar.com

INTERNATIONAL JOURNAL OF ADVANCED RESEARCH (IJAR)

Article DOI:10.21474/IJAR01/16305
DOI URL: http://dx.doi.org/10.21474/IJAR01/16305

RESEARCH ARTICLE

EFFECT OF PHASE TRANSFORMATION ON OPTICAL PROPERTIES OF ZNTIO$_3$ CERAMIC POWDER PREPARED BY SOL-GEL METHOD"

Aiyeshah Alhodaib, S. Abdel Aal and Mashael Khaled Abdulaziz Alnasser

Manuscript Info

Manuscript History
Received: 15 December 2022
Final Accepted: 19 January 2023
Published: February 2023

Abstract

$ZnTiO_3$ powders were prepared by sol-gel method using ammonium hydroxide. The effects of calcination temperature (500– 1000◦ C). and the molar ratios ZnO/TiO2. The synthesis of a nano perovskite ZnTiO3 usually results in the formation of one or more of the compounds such as Zn2TiO4, and ZnTiO3 with other secondary impurity phases such as rutileTiO2 or ZnO. To obtain a phase-pure a nano perovskite ZnTiO3 at a low processing temperature is one of the challenges in materials chemistry., pure ZnTiO3 can not be synthesized under normal conditions, because it transforms into Zn2TiO4 and rutile. In the current study, the crystalline and phase transformation behaviors of sol-gel synthesized a nano perovskite ZnTiO3 has systematically been investigated with regard to various Zn:Ti precursor molar ratios. The $ZnTiO_3$ phase can be detected by XRD in the powders calcined above 600 °C. The formation of $ZnTiO_3$ is a slow reaction process, which leads to the development of large $ZnTiO_3$ particles, with dimensions after calcination at 700 °C for 5 h in the range of 68–81 Nm. Calcination temperature increased considerably the crystallite size of the nano perovskite ZnTiO3 from 68 to 81 nm This treatment led also to the creation of holes in the matrix of calcinated solids which increased the mobility of charge carriers (electrons) leading to a significant decrease in the decrease in the optical energy gap reaching to (2.7 to 2)e.v.

Copy Right, IJAR, 2023,. All rights reserved.

Introduction:-

The development of ceramic and semiconductor oxide materials is helping to meet the growing demand in industrial and laboratory applications. they demonstrates excellent dimensional stability and can be manufactured to meet precise tolerances. Its strength and temperature resistance, combined with high resistivity and dielectric strength, make it an attractive alternative.1

Fundamental studies concerning the phase diagram and characterization of ZnO-TiO2system have been published since 1960s. This system still attracts the attention of researchers because of its importance in practical applications.Evolution of highly ordered inorganic metal oxide nanostructures has gained substantial momentum in recent years, owing to their extraordinary structural and electronic properties. The tremendous increase in the demand for nanoscale electronic devices[1,2] has motivated researchers to produce complex functional nanomaterials consisting of binary and/or ternary composites in addition to pure phases.2. Among many photocatalytic materials, ZnO has attracted extensive research attention due to its low cost, good chemical stability, and high electron

Corresponding Author:- Aiyeshah Alhodaib

mobility [3,4,5]. Pure ZnO will encounter some problems when it is directly applied to photodegradation. The forbidden bandwidth of ZnO is large (Eg = 3.37 eV), which can only absorb a small amount of ultraviolet rays in the sunlight. On the other hand, the photogenerated electrons generated by excitation are apt to reunite with holes [6,7,8 ,9]. Therefore, combining ZnO with other semiconductors to form heterojunctions is helpful to generate more free radicals and improve the photodegradation effect [10]. The most studied ZnO semiconductor systems are ZnO/ TiO_2 [1,11]

TiO_2 ceramics have been investigated for diverse applications in the optical and semiconductors industries because of their interesting semiconducting and dielectric properties. Semiconducting titania had especially been employed in producing different electronic devices, including oxygen sensors, varistors, and current collecting electrodes in Na-S batteries [6–8].

TiO_2-ZnO-based compounds have been employed as promising catalysts in some chemical industries

Currently, zinc titanates have found practical applications as dye pigments (McCord and Saunder, 1945), materials for radioelectronics (Kagata et al., 1993; Kim et al., 1998a, 1998b; Kim et al., 1999), gas sensors (Yadava et al., 2013; Obayashi et al., 1976), catalysts (Chen et al., 1996; Kong et al., 2009; Wang et al., 2012) and sorbents for desulfurization (Swisher et al., 1995; Lew et al., 1989; Susan et al., 1992). Research on their synthesis is still relevant because of its importance in practical applications (Steinike and Wallis, 1997; Hosono et al., 2004a, 2004b; Liua et al., 2009).

Kong et al., synthesized and characterized perovskite $ZnTiO_3$ photocatalysts. They investigate that the perovskite $ZnTiO_3$ could serve as a potential photocatalyst to decompose emerging contaminants. In fact, perovskite ZnTiO3 is also used in a wide array of applications, such as on gas sensors, microwave dielectrics, and sorbents; therefore, it is critical to develop a facile method to fabricate $ZnTiO_3$.

ZnTiO3 is of a perovskite type oxide structure and could be a useful candidate as microwave resonator [7], gas sensor [8] (for ethanol, NO, CO, etc.), microelectronics [9], metal-air barriers [10], and as high performance catalysts [11, 12] for the complete oxidation of hydrocarbons or CO and NO reduction [13] and paint pigment [14].

From the work of**Praveen K. Jain** et al, Various parameters were optimized in order to achieve single phase ZnTiO3. Here, the effect of sintering temperature on the energy band gap has been investigated. It was found that the sample sintered at 800 °C for 12 hour exhibit single hexagonal phase of $ZnTiO_3$. The indirect band gap of samples sintered at different temperature ranging from 700 °C to 1000 °C was calculated from absorption spectra, which reveals that band gap is minimum for single hexagonal ZnTiO3 phase (2.88 eV) as compared to mixed cubic/hexagonal phase (2.91 eV).

It is well known that the properties of materials depend on their synthesis processes and calcination conditions. For ZnTiO3, its physicochemical properties are influenced by their preparation conditions. In general, there are some methods to prepare ZnTiO3 powder, including conventional solidstate reaction [1], sol-gel method [15], ..., and so forth. The solid-state reaction method has some drawbacks including high temperature, large particle size, and limited degree of chemical homogeneity. The chemical solution methods can provide products of fine and homogeneous particles with high specific surface area. The processing of complex oxide ceramics using sol-gel techniques has been extensively studied [16–20] The Pechini method is a conventional approach to prepare powder consisting of oxides of transition metals. This method requires first dissolution of hydrous oxides or alkoxides of element in polyhydroxy alcohol such as ethylene glycol, with a chelating agent, such as citric acid. Subsequently thermal treatment is performed at relatively low temperatures leading to the formation of highly homogenous powder [21].

In this paper, the authors have attempted to prepare nano perovskite $ZnTiO_3$ ceramic materials by sol-gel method. The role of calcination temperature and molar ratio of the obtained solids on their structural and optical properties were investigated. The techniques employed were TGA, XRD, UV.

Fundamental studies concerning the phase and the characterization of the ZnO–TiO_2 system have been done, and five compounds often exist in the ZnO–TiO2 binary system including $ZnTiO_3$ (cubic, hexagonal), Zn2TiO4 (cubic, tetragonal) and Zn2Ti3O8 (cubic) [16–18].

Experimental

Materials. certain amounts of ZnClO4 and TiClO4 with stoichiometry (Zn/Ti = 1 : 1.3:7and 7:3) were dissolved in distilled water stirred for 3 hours. NH4OH solution was added dropwise to mixed solutions as a precipitating agent. The precipitation process was carried out at room temperature and a pH of about 8. The precipitate was dried at 70∘ C for 4 days and the large agglomerates were pulverized in an agate mortar. The ceramic materials was obtained after heating in air for 5 hours at temperatures between 500-900C

Systematic studies concerning the role of calcination temperature and molar ratio on structural and optical properties of the treated solids were investigated.

Thermo gravimetric analysis(TGA) measurements were carried out by Shimadzu instrument (DTA-50) calibrated through the melting points of indium and tin. The thermogravimetric analysis (TGA) was recorded using the (TGA50) system in the presence of air, within a temperature range from room temperature up to 800∘ C at a heating rate of 30∘ C min^{-1}.

Techniques. X-ray powder diffractograms were carried out on samples calcined at temperatures within 500 and 900∘ C were obtained using a Bruker diffractometer (Bruker D8 advance target). The patterns were run with Cu Kα1 with secondly monochromator (λ = 1.5405A) at 40 kV and 40 mA. The crystallite size ˚ of crystalline phases present in different solids investigated was calculated from line broadening profile analysis of the main diffraction lines of crystalline phases present using the Scherer equation [18]:

$$\mathrm{d} = \frac{\mathrm{k}\lambda}{\mathrm{B1/2}}\cos\theta$$

where d is the mean crystallite diameter, λ is the wave length of X-ray beam, K is the Scherer constant (0.89), β1/2 is full width at half maximum {FWHM} of the main diffraction peaks in radians, and θ is the diffraction angle.

Optical techniques such as U.V. absorption and photoemission can be used on prepared samples in the range of wave length 300-1500 Nm

Results And Discussion:-

Thermal Behavior of $ZnTiO_3$ Powders

It is well know that the sol-gel technique has the unique advantage of providing extremely small and uniform particle size for the precursor powders. The prepared powders were analyzed using TGA for burnout behaviors. Figure 1 shows TG curve of the prepared non calcined mixed solids, being dried at 70∘ C and having equimolar ratio of ZnO and TiO_2 existing as an amorphous powder. The TGA curve shows Initially, a weight loss of 12.9% was observed before 200 ◦C in the first stage, mainly due to the evaporation of the amonia solvent [22]. A weight loss of 40.5% occurred from 200 to 500 ◦C in the second stage. In the second stage as well, thermal decomposition with a maximum weight loss of 31.4% was observed at 315 ◦C. the dihydroxylation of Ti-OH to TiO_2 occurred in this stage. The weight loss in the third stage between 500 and 800 ◦C reached 42.4%, and the weight loss increased by approximately 2%, indicating that the residual organic components had been burned out. Since the TGA curve did not change much after 500 ◦C, this suggested that the samples had to be calcined above this temperature at least to remove the organic precursors.

Accordingly, the thermal post-treatments of the as-prepared $ZnTiO_3$ samples were set at 500, 600, 700,and 900 ◦C.

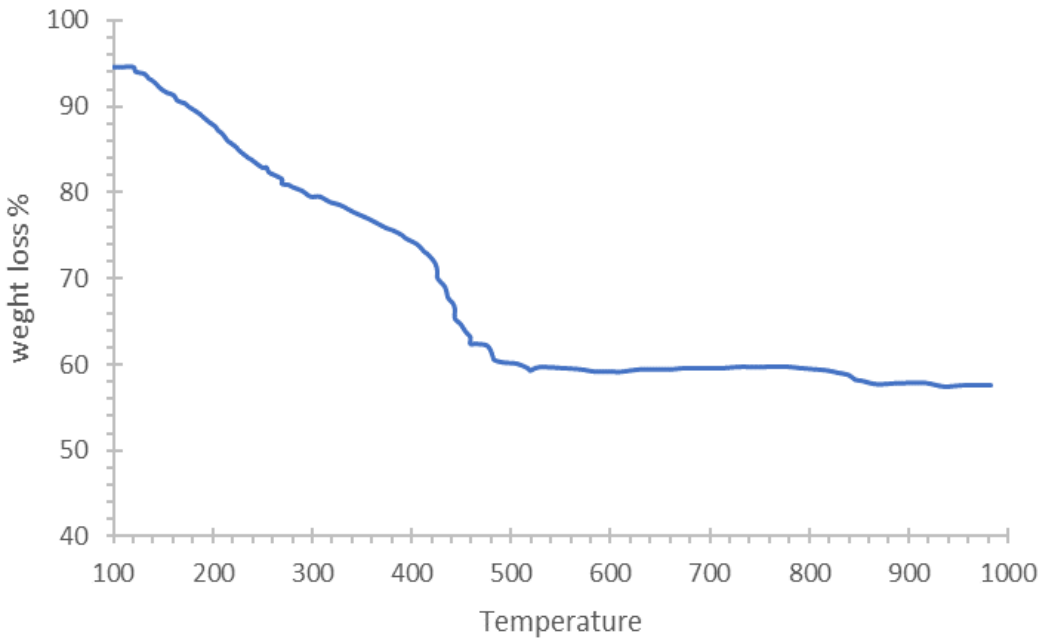

Figure 1:-TGA of the amorphous prepared powder.

XRD Investigation of ZnO/TiO2 System

Calcined at Different Temperatures. X-ray diffractograms of ZnO/TiO2 system calcined at 500, 600, 700, and 900◦ C were determined.

The XRD patterns of the amorphous powder prepared ZnTiO3 at various calcination temperatures are shown in Figure 2. For the case of 400 ◦C, the signal of the XRD pattern was not sharp.

These were weak and broad peaks, such as 30.1◦ (220), 35.2◦ (311), 42.4◦ (400), 53.3◦ (422), 56.9◦ (511), and 61.8◦ (440), indicated the existence of cubic Zn2TiO4 (JCPDS 25-1164).

This also indicate that the calcination temperature of 400 ◦C was not enough for the crystallization of ZnTiO3

As the calcination temperature reached 600 ◦C, several peaks including 14.9◦ (110), 23.6◦ (210), 26.0◦ (211), 30.0◦ (220), 35.3◦ (311), 43.0◦ (400), 53.3◦ (422), 56.9◦ (511), and 62.4◦ (440) were observed, representing the formation of cubic-phase ZnTiO3 (JCPDS 39-0190).

The strength of these peaks increased even more rapidly at 700 ◦C. As the temperature of heat treatment increased further, the cubic phase of ZnTiO3 was transformed into the hexagonal phase at 800 ◦C [48]. The characterized hexagonal phase was verified from the 2 θ of 19.15◦ (003), 23.9◦ (012), 32.7◦ (104), 35.3◦ (110), 38.8◦ (006), 40.5◦ (113), 50.3◦ (107), 53.4◦ (116), 56.8◦ (018), and 61.8◦ (214) (JCPDS 26-1500). On the other hand, the XRD pattern also revealed that the cubic-phase ZnTiO3 was partially decomposed into cubic Zn2TiO4 at 800 ◦C. Accordingly, the different calcination temperatures had a significant impact on the crystallinity of ZnTiO3.

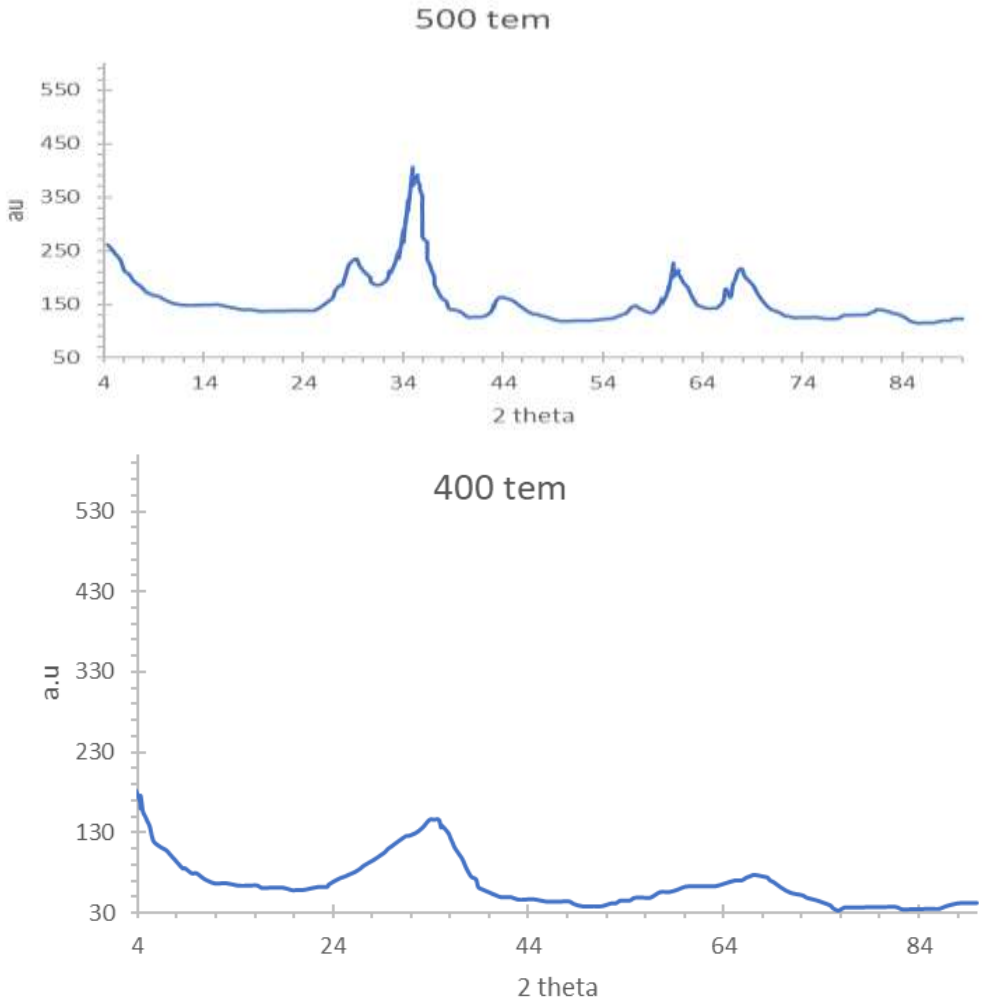

Fig 2:- XRD pattern for prepared powder at 400and 500^{0}C.

The effect ofmolar ratio of the Zn/TiO2 on the prepared samples

Fig 3 illustrates the XRD pattern obtained for X Zn (100-X) TiO_2 with X=30,50 and 70% weight after heat treatment at 600^{o}C for 5hrs. During the calcination the rearrangement of atoms within the crystal lattice has been occurred to produce homogeneous compound, according to the thermo-gravimetric analysis the samples with different ratio with the system X Zn (100-X) TiO_2 to select the best ratio for preparation $ZnTiO_3$.

In pattern of XRD the samples with composition 30Zn/70TiO_2 the major component is The main peaks are related to TiO_2 with Anates phase at position at position 2ɵ= 25.27,38.52,48.1,55.03,62.5 and Rutile phase at position 2ɵ= 27.4,41.2,56.6 and 69.1 in addition to some peaks of $ZnTiO_3$ shown in the pattern with low intensity and some intermediate phases from the first ingredients such as ZnO position at position 2ɵ=34.42,47.5 are formed.

The variation of molar ratio does not influence on the formation of cubic and hexagonal $ZnTiO_3$ phase with a minor amount at position 2ɵ= 35.3 and32.82 respectively with low intensity; At ratio 30ZnO/70TiO_2, .

The diffracted lines with 2ɵ=34.42, 36.1, 47.53, 56.6, and 66.4^{0}indicating the presence ofZnO as major component in samples with ratios 70ZnO/30TiO_2 along with minimum amount of the two phases of $ZnTiO_3$ at 2ɵ= 35.3, 32.8 and Anatase TiO_2 at 2ɵ= 25.4.

The major diffracted lines at position 2ɵ= 30, 35.2, 43, 53.3,56.9 and 62.4^o in sample with ratio 50ZnO/50TiO_2 indicate to presence the cubic $ZnTiO_3$ as the main component.

Despite the fact of our aim to prepare cubic $ZnTiO_3$ and study the phase transformation of the prepared compound that would exhibit unique photocatalysis properties and best compatibility to be used in different medical application we have reached to an interesting physical properties, in particular, ratios of ZnO/TiO_2 content has dramatically effect on the formation of the $ZnTiO_3$ phase .The formation of cubic phase $ZnTiO_3$shown the strongly ratio dependent, and this agree with(Chemical Synthesis and Characterization of ZnTiO3 Powder Prepared by the Coprecipitation Oxalate Method)

The patterns of XRD show that the ratio $50ZnO/50TiO_2$ is considered to be the optimum ratio because most of ZnO and TiO_2 content share in formation of cubic $ZnTiO_3$except some diffracted lines of ZnO and TiO_2 at $2\theta=47.54^0$ and $2\theta=54.8,69.1$respectively. The presence of these diffracted lines can be attributed to several factors as chemical effects or need more sintering sintering temperature time .

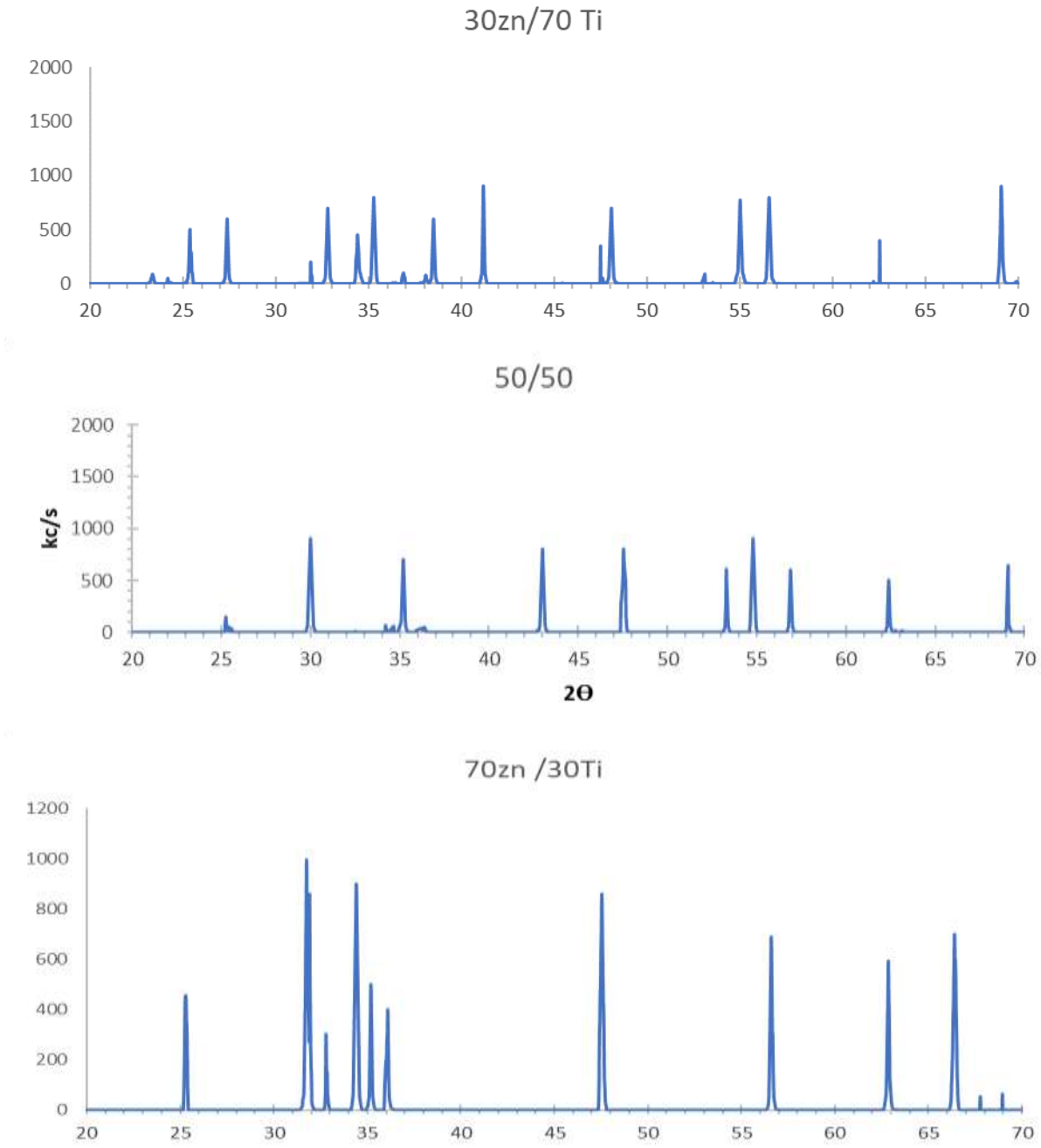

Fig 3:- Effect of molar ratios on the formation of $ZnTiO_3$ sintering at 700^0C.

Effect of sintering temperature on the samples with ratio 50/50

Figure 4 shows the XRD patterns of $ZnTiO_3$ powder prepared by the sol-gel methodcalined at (a) 500 °C (b) 700 °C and (c) 900 °C for 9h. At lower calcinations temperature, 500 ^oC for 9h, the XRD pattern shows a mixture multiphaseofZnO at 31.77, 34.428, 47.58 and 56.608, with (100),(002) ,(102)and (110) corresponding to ZnO (JCPDS no. 36–1451), indicating to the formation phase of ZnO was wurtzite in addition to the prediction lines indicating to the formation $ZnTiO_3$ with cubic structure at 26.0 ,30, 35.3 and 43.0 with and (Fig. 3.3) corresponding to the JCPDS File Card No. 05-0664 [14] and 30-0190 [12], respectively and broad peak of TiO_2 with anatase phase at 62.5 ^oC. At calcinations temperature, 700 ^oC for 5h, the XRD pattern shows a mixture multiphase of TiO_2 with anatase and $ZnTiO_3$ with cubic structure (Fig. 1. (b)) corresponding to the JCPDS File Card No. 12-1272 [15] and 30-0190 [12], respectively. At calcinations temperature, 900 ^oC for 9h, the XRD pattern shows a mixture multiphase of $ZnTiO_3$ with cubic and dominant $ZnTiO_3$ with hexagonal structure 23.9, 38.8, 40.5 at (Fig. 3.3) corresponding to the JCPDS File Card No. 30-0190 [12] and 14-0033 [13], respectively. The intensity of ZnTiO3 peaks increased with increased calcination temperature.

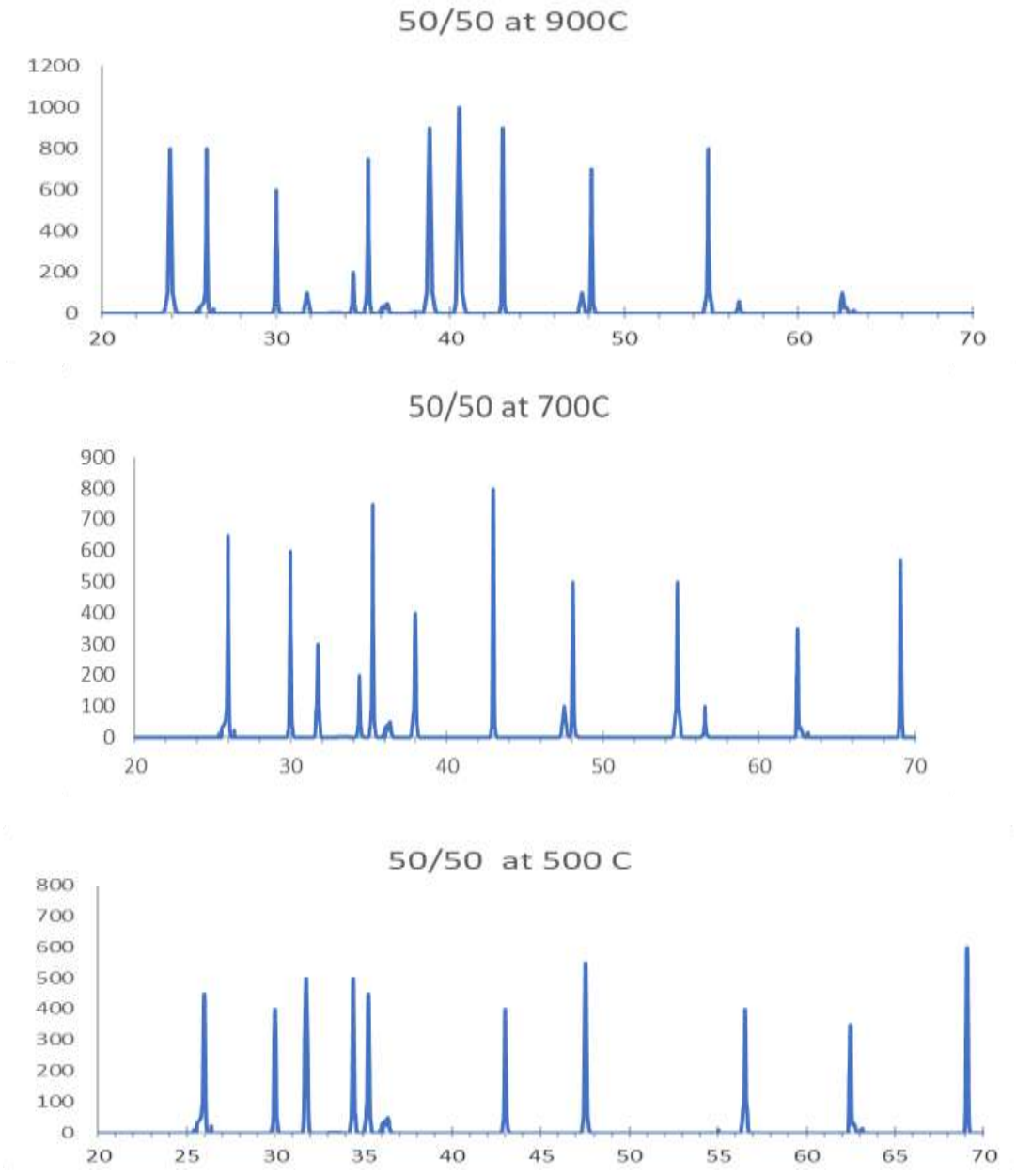

Fig4:- Effect of sintering temperature on the samples with ratio 50/50.

The average crystallite size was determined from the XRD powder pattern according to the Scherrer's equation [17]

$$D = k\lambda/\beta\cos\theta \qquad 3.2$$

where D is the average grain size, k is a constant equal to 0.9, λ is the X-ray wavelength (0.1542 nm), β is full width at half maximum, and θ is diffraction angle

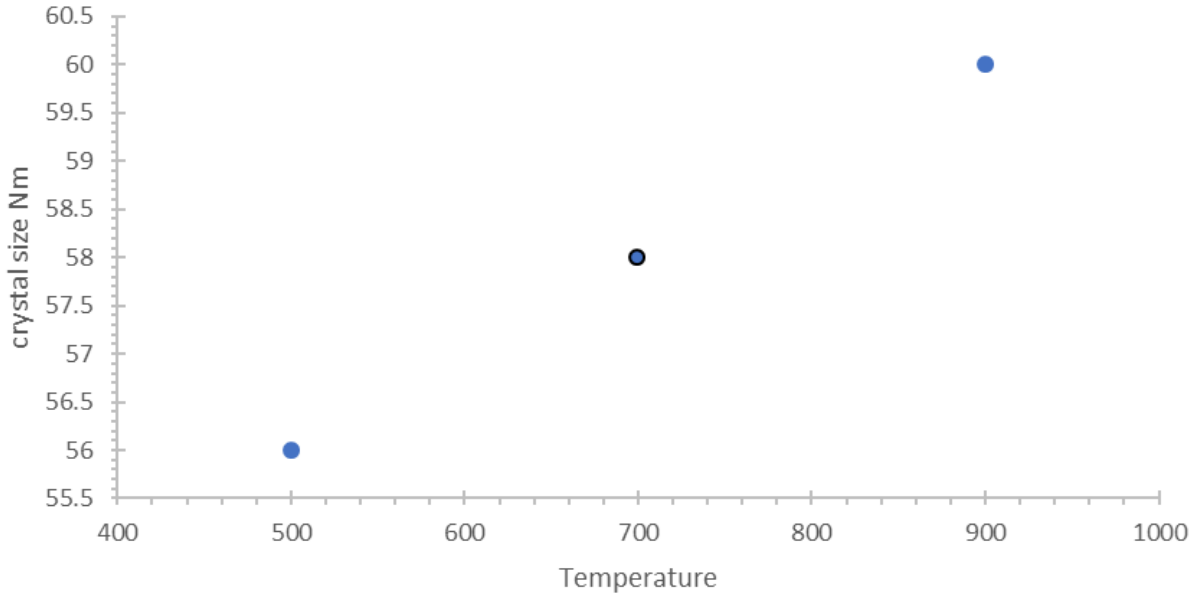

Fig5a:-Effect of calcinated temperature 500,700and 900^{0}C on the crystal-size of prepared samples.

Figure 5.a presents the behavior of crystallite size. The crystallite size depended on the lattice micro-strain. It has been observed that generally the average crystallite size increase with the increasing the temperature, and this may be attributed to the growth of the crystal structure.

A W–H (Williamson–Hall) plot is a very important technique for measuring the values of lattice parameters and crystallite size as well. Equation (2) was used to plot (W–H) graphs for all the samples [25]

$$\beta\cos\theta = \frac{\lambda k}{D} + 4\varepsilon\sin\theta$$

where $'\beta'$ is the full width at half maximum (FWHM), $'\theta'$ is the Braggs angle, $'k'$ is the size factor=0.98, $'\lambda'$ is the wavelength of X-rays=1.504, and 'D' is the average crystallite size. Finding the slope of a linear plotted graph against $4sin\theta$ gives the information about the lattice strain and crystalline size (DW–H) for all the samples as shown in figures 5.the effective values of crystallite size (DW–H) were measured by the Williamson–Hall (W–H) technique, and were found 81,73 and 68 ,it was very close to the values which got from Arrhenius equation.

The average values of crystallite size (DW–H) and micro-strain (εW–H) along with uncertainties were measured by the Williamson–Hall (W–H) technique, as shown in Table 1. Around the fitted line, the points are noticed to be widely scattered. It was observed that certain additional parameters of the characterized samples were not taken into consideration.

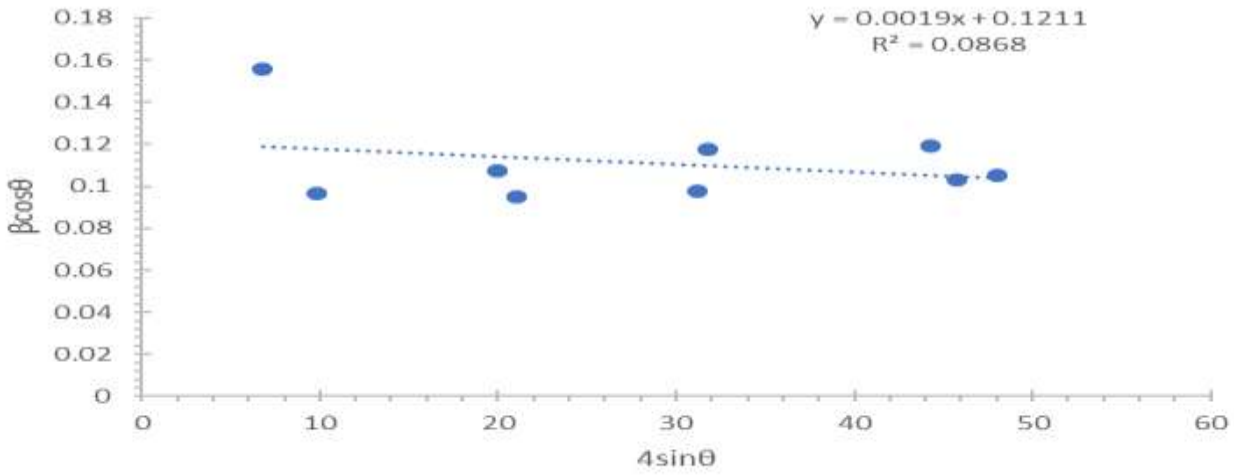

Fig 5.b:-The macrostrain of sample calcinated at 900 ^{0}C.

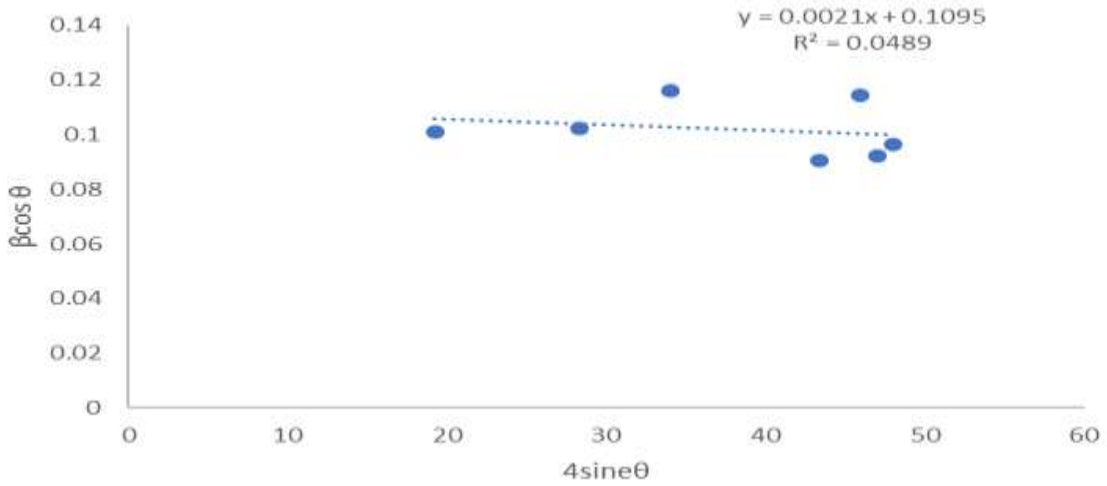

Fig 5c:-The macrostrain of sample calcinated at 700 ^{0}C.

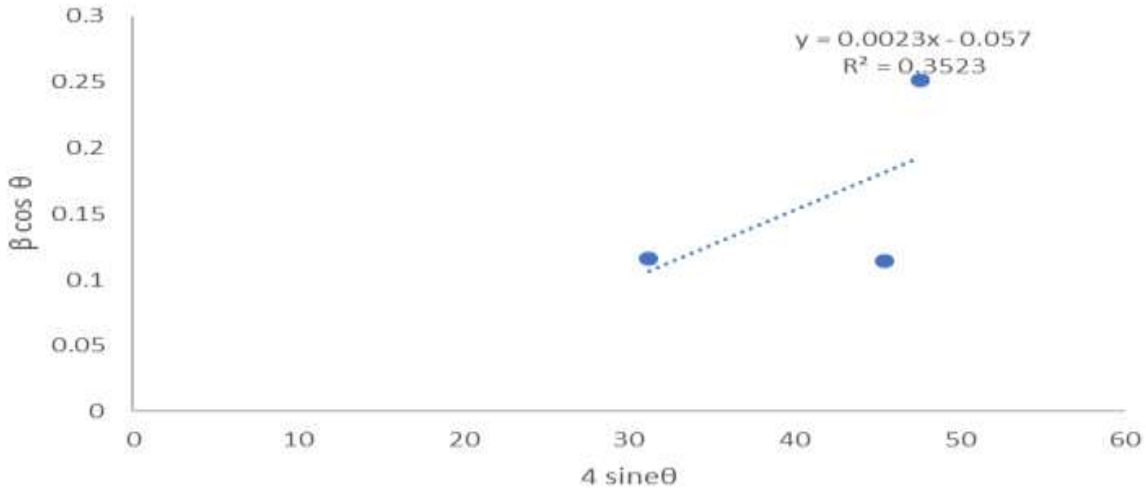

Fig 5.d:-The macrostrain of sample calcinated at 500 ^{0}C.

Effect of sintered temperature on the molar volume and the density

The temperature of an object varies with the changes in the density of this object. The mass of a particular object is eventually compared to the objected volume. The equation of density is important to understand the relation of temperate with this component (Bertini et al. 2021).

The formula is Density = mass/volume

This formula can also be presented as D = m/v. The size of the mass plays an important role in changing individual density. In different temperatures, the atoms and arrangements of an object are found to change accordingly.

There are two different types of density namely relative density and absolute density (Fable et al. 2019). The changes in temperature impact both of these types of density.

The molar volume (V_m) of the ceramic samples can be calculated from the following formula:

$V_m = M/\rho$ (1)

Here, V_m is the molar volume, ρ is the density of the sample and M is the molecular weight of the sample. Each calculation may be demonstrated here for samples of nano perovskite $ZnTiO_3$. The results obtained in the case 50%/50% of of nano perovskite $ZnTiO_3$ samples are summarized in the Table (1) as well as shown in fig..6a, b) and fig. 7

From fig. 6 a, b and fig. 7 The values of the density and volume increasing from 4.52to 5.306 g/cm^3 ; while the values of the molar volume is decreasing from 35.66 to 30.38 cm^3 with the gradual increase of the calcinated temperature on of nano perovskite $ZnTiO_3$. The variation of density and molar volume with calcinated temperature of nano perovskite $ZnTiO_3$ for all samples is due to formation of perovskite $ZnTiO_3$. which results in decreasing of the values of optical energy gap (Eg), accordingly the electrical conductivity increased, as shown in the optical results and energy gap values

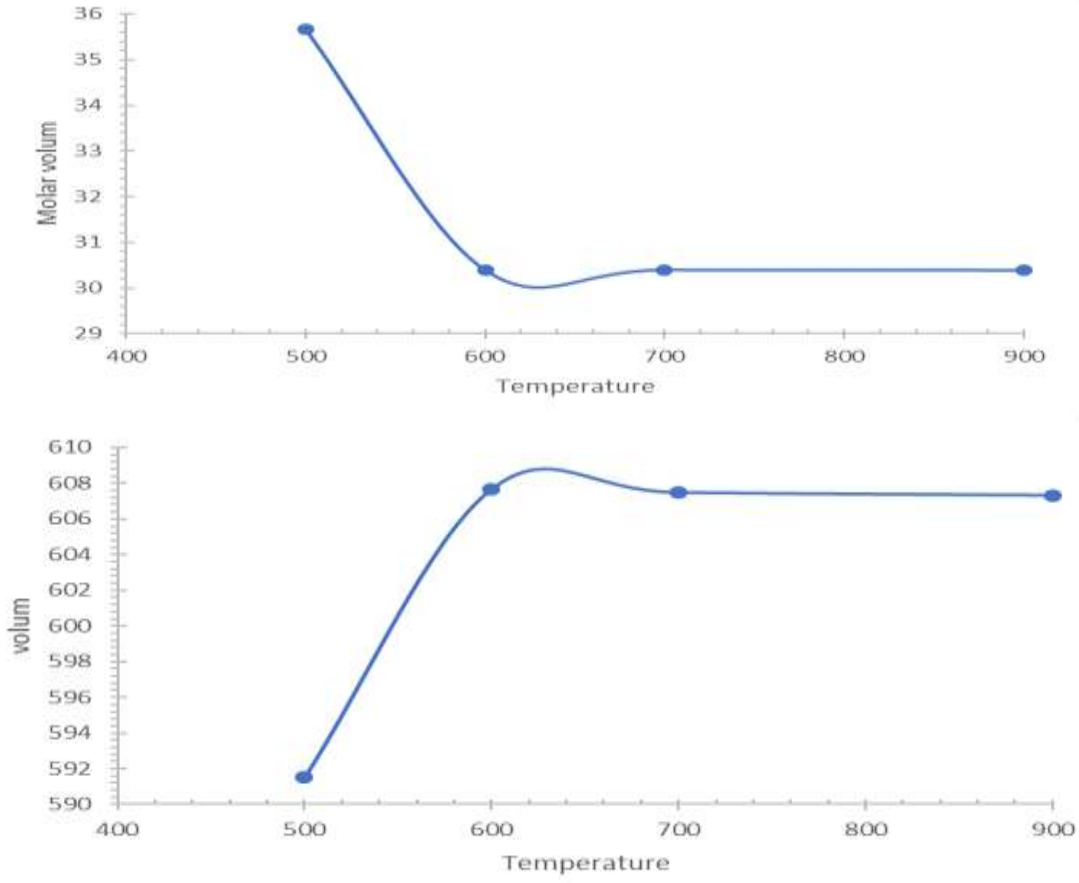

Fig.6 a, b:- Effect of temperature on the Molar volume and unit volume cell.

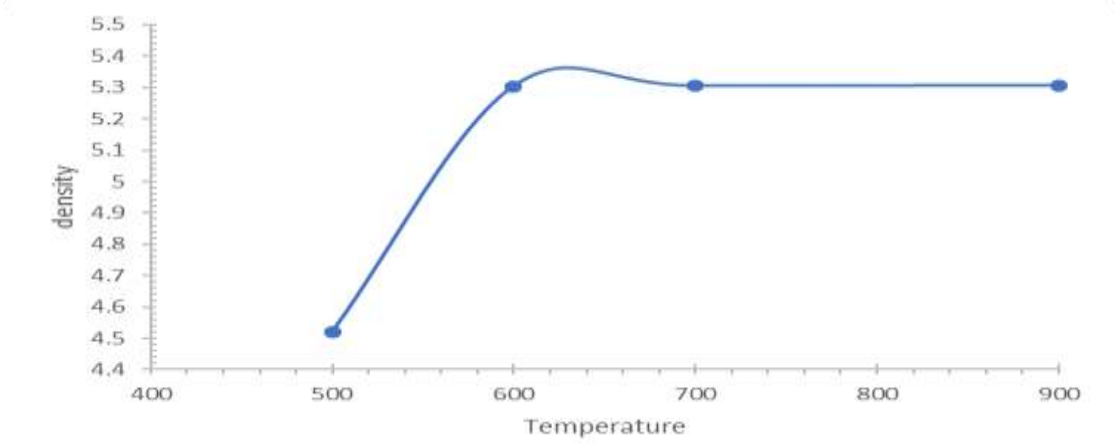

Fig.7:- Effect of calcinatedtemperature on density of prepared samples.

Table 1:-Data on (DW–H) and (εW–H) of calcinated $ZnTiO_3$.

samples	Crystal size Arrhenius eqNm	average crystal size	Crystal size D_{wH}	Micro strain D_{wH}	Unit cell volume $V(A)^3$	CalculatedDensity (g/cm3)	Molar volum Vm
500C	68	68	66.999nm	0.0023	591.49	4.52	35.66460177
600	69	75	73.33nm	0.0021	607.62	5.304	30.39291101
700	77	78	81.05nm	0.0019	607.43	5.305	30.3871819
900	78	79	81.05	0.0019	607.22	5.306	30.38145496

UV–visible spectrophotometric measurements

ZnTiO3 have been synthesized via the facile sol-gel route in varying molar-based sol ratios of Zn:Ti (v/v).

In general, the spectrophotometer is working in the solar radiation region, its measurement is either Transmittance (T) or reflectance (R) of the samples.

The absorbance is not measured directly but is calculated from the measured T and R. When spectrophotometer gives the absorbance A on the log form,

the optical density OD =log 10/T =α X

where: X is the penetrating length or the depth, T is transmittance and α is absorption coefficient (lamber law).

Optical properties of materials depend on many parameters, such as the preparation technique, the preparative conditions and surface morphology. The study of the spectral behavior of the absorption coefficient of any semiconducting material gives good information about the electronic states in the high energy part of the optical absorption spectrum, while the other lower energy part of the spectrum corresponds to the atomic vibrations [26,28] F. Urbach, Phys. Rev. 92 (1953) 1324.

[26] M. El-Hagary, M.E. Ismail, E.R. Shaaban, A. El-Taher, Rad. Phys. Chem. 81 (2012) 1572. . There are several applications based on the optical absorption of of ZrTiO3like photovoltaic, optoelectronics, sensors, display devices, solar cell, photo-electrochemistry,……..etc . For all these reasons, the optical absorption spectra and the optical absorption coefficient (α) should be studied. The absorption coefficient α can be determined from the equation

$$\alpha = 2.303\ (A/t)$$

where t is thickness and A is the absorbance

The dependence of the optical absorbance coefficient, (α) of ZrTiO3upon the incident wavelength for the lower calcinated and higher calcinated samples is shown in Fig 8. From the analysis of Fig. 8 we can show that, the value of absorption coefficient (α) decreases with the increase in the incident wavelength for all the samples of $ZrTiO_3$.

In Near -IR region, the values of (α) decreased by increasing the wave length. This is due to the absorbing nature of the element. It has been also observed that, the absorption coefficient, (α) has values for the samples in the order of

10^1 cm^{-1} in all samples.The UV patterns for both non-calcinated and calcinated compound $ZnTiO_3$ were shown in Figure.8.b). The slight high intensity absorption peak of both the non-calcinated and calcinated samples in the UV section concentrated at 420 nm (2.95 ev) could have resonance with transition within this band gap (band-to-band) and formed via the oxygen vacancies, due to formation $ZnTiO_3$ from TiO_2 and ZnO this agree with [27]. The Transmittance peaks in fig.9 were remarkably elevated with the elevation of the temperature and shifted to some extent to shorter wavelength redshift This could be explained by the fact that the optical properties of oxides are directly affected by the higher temperature such as oxygen vacancies that causes lattice distortion in its direct surrounding and this confirmed by XRD. and indicated and confirmed the decreasing of optical band gap (E_g^{opt}) with increasing the temperature. These obtained results are in good agreement with other previous works [8,28,29,16,17 .

Figure 9 and 10 show the optical transmission and reflection as a function of photon energy hn for $ZnTiO_3$ in different sintering temperature

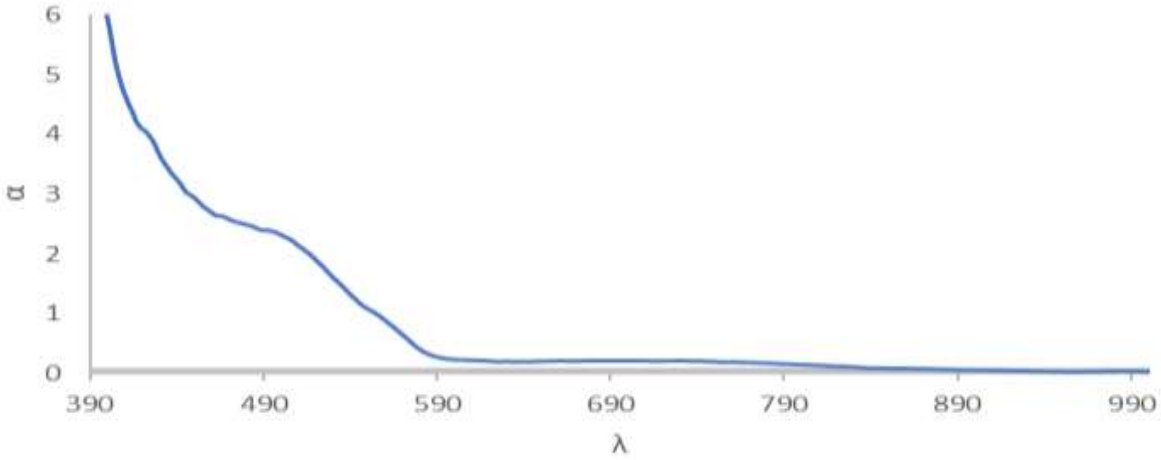

Figure 8a:-The absorption coefficient with the wave length of the prepared sample.

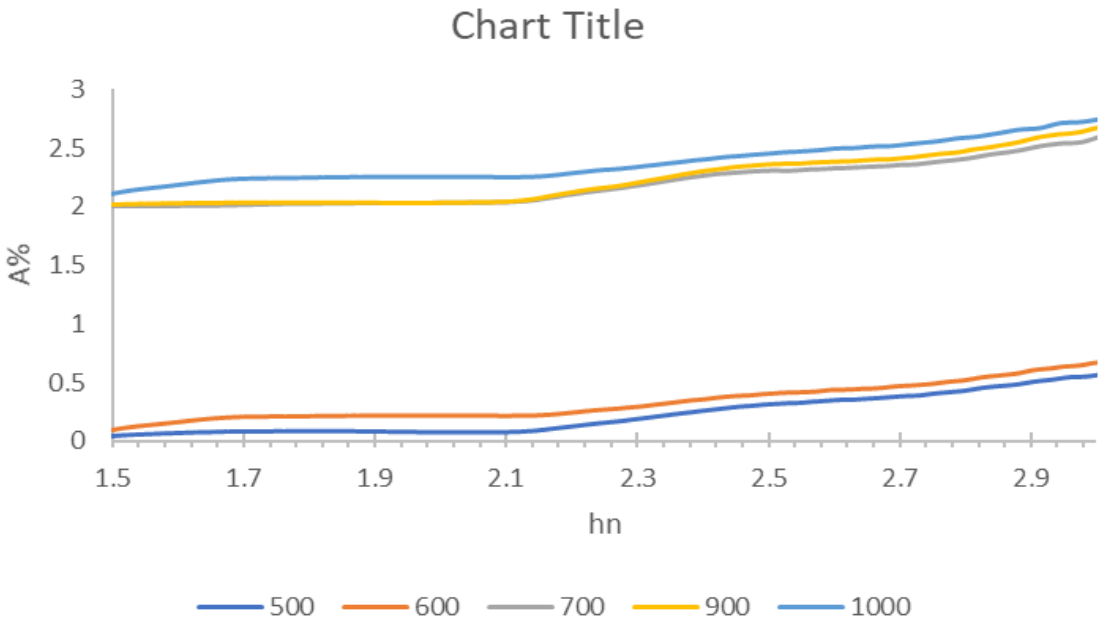

Figure 3.8.b:- UV absorption of the prepared samples with incident photon energy e.v.

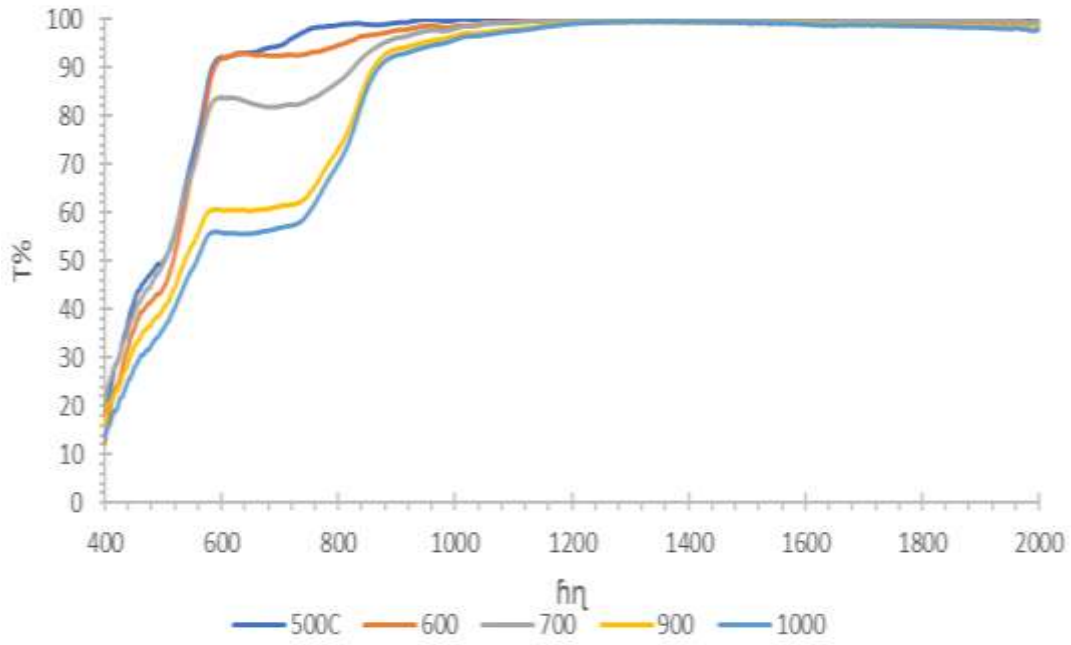

Figure 9:- Effect of calcinated temperature on the T% pattern of prepared samples.

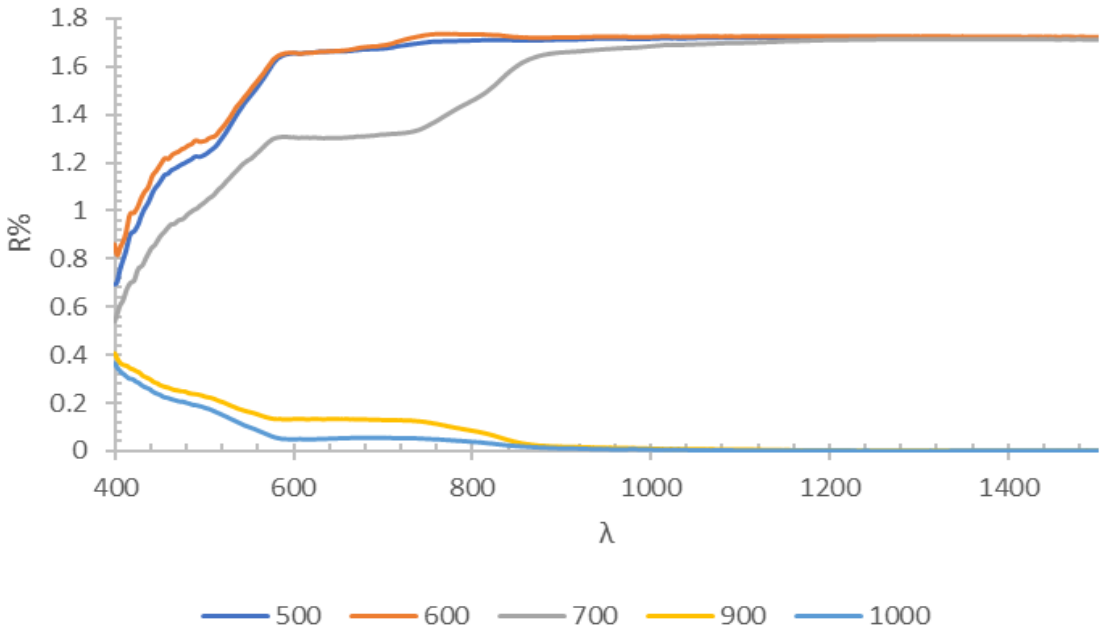

Figure 3.10:- Effect of calcinated temperature on the R% of prepared samples

Figure 11 shows the plot of refractive index (n) versus energies (eV) of ZnTiO3 s. Refractive index was calculated using the following equation [21]:

$$n = \sqrt{1 - R} / \sqrt{1 + R} \qquad 3$$

where R is the reflectance. It could be seen that ZnTiO3 film had the highest refractive index (1.0 ~1.3) at lower energies (E < 2.5 eV) and the refractive index decreased gradually to less than 1.2 at higher photon energies (E > 2.8eV), especially for samples calcinate at higher temperature.

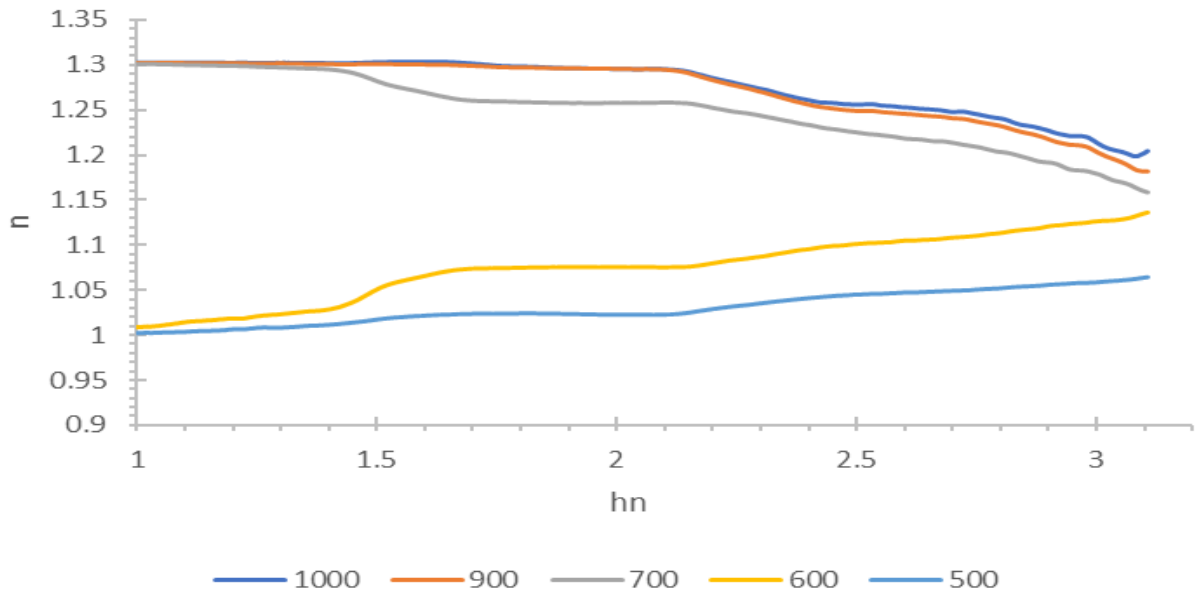

Fig (11):-Effect of calcinated Temperature of the perovskite $ZnTiO_3$ on refractive index.

The optical band gap energy Eg may result from a plot of photon energy hυ against (αhυ), as in Figure.12. The (αhν) against (hν) plots of perovskite $ZnTiO_3$is linear over a wide range of photon energies, as demonstrated in figure 12. This specifies the incidence of a direct optical band gap in the specimens agree with[23].

Optical band gap of these was attained by extrapolation of linear portion (αhυ)to cut x axis hυ provides Eg.The results are demonstrated in Table 2 that the optical band gap of the composite decreases with calcinated temperature due to the formation of perovskite $ZnTiO_3$ induce slightly defect and this confirmed by the result of XRD and agrees with the results reached by [24].

The optical absorption spectra of perovskite $ZnTiO_3$ have an important role because it gives the basic information about its composition and its optical band gap. The optical absorption spectra of the materials can be divided into three main regions; they are (1) weak absorption region, which arise from defects and impurities, (2) absorption edge region, which arise due to perturbation of structural and disorder of the system and (3) the region of strong absorption that determine the optical energy gap. The exponential area situated in close proximity to the edge of optical band is referred to as Urbach tail. Typically, it is observed in amorphous, disordered and materials with insufficient crystalline owing to localized states found within the gap of the band [24][25]. In the low photon energy range, the spectral dependence of the absorption coefficient (α) and photon energy (hυ) is known as Urbach empirical rule, which is given by the following equation [34]:

$$\alpha = \alpha_0 \exp\left(h\upsilon/E_u\right) \qquad 4$$

In the equation above, α_o denotes a constant with E_U signifying the Urbach energy. This energy slightly depends on temperature. In addition, it is always marked using the band tail width due to localized states within the normally band gap linked to the disordered crystalline materials [29,32,34]. It is noteworthy that the straight-line equation can be concluded from the ln of both sides of eq 4:

$$\ln \alpha = \ln \alpha_0 + (h\upsilon/E_u) \qquad 5$$

It is possible to calculate Urbach energy (E_U) can from the plotting's straight line (slope) ln (α) versus (hυ), which is the energy of incident photon, as demonstrated in figure.13.

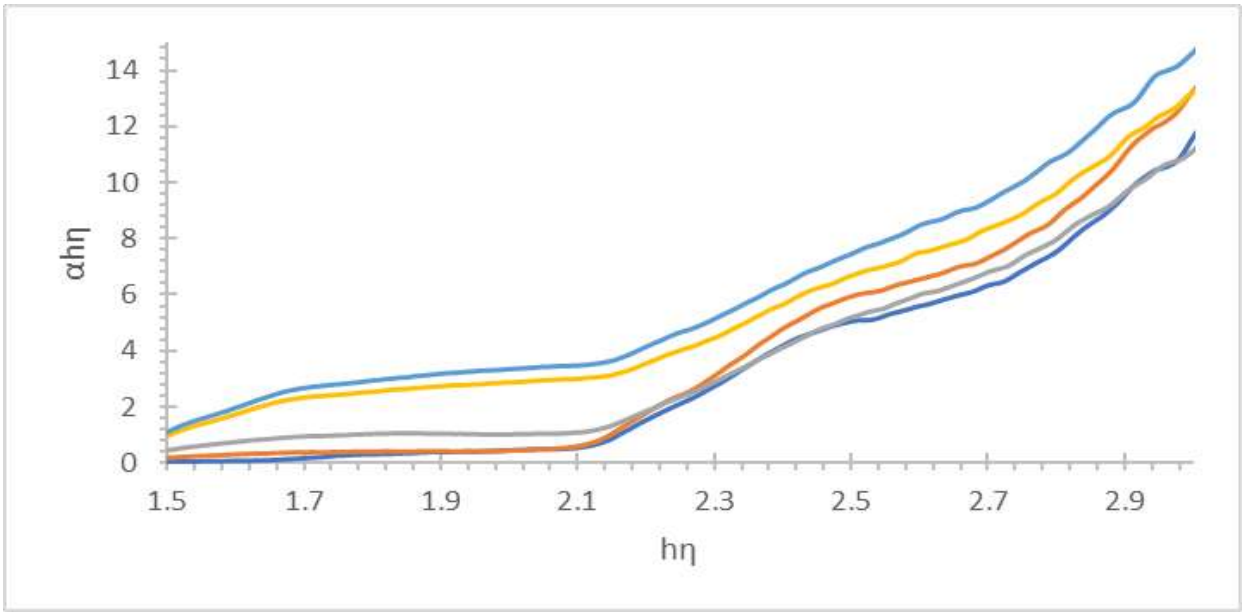

Fig. 12 a:-Plot of photon energy hυ against (αhυ).

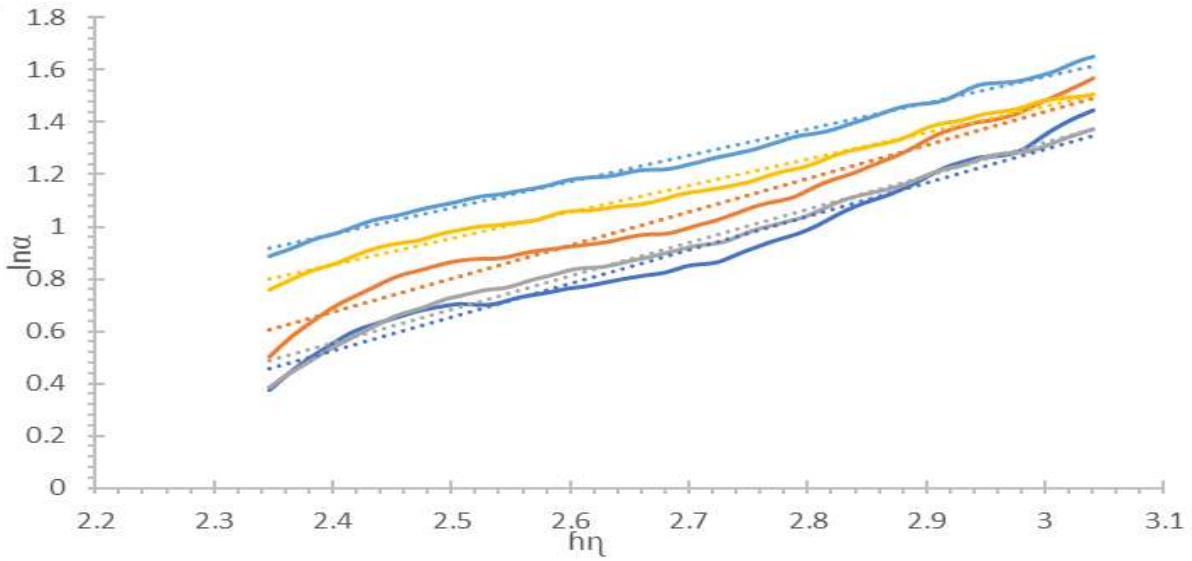

Figure 13:-Urbach energy (E_U) can from the plotting's straight line (slope) ln (α) versus (hυ) band tail.

From figure 12 The optical energy gaps (Eg) were determined from the optical absorption curves using the imperial equation [20]:

where A is a constant, ν is the frequency of the incident radiation and h is the Planck's constant. It is known that, the exponent p = 1/2 for allowed direct transition, while p = 2 for allowed indirect transition. Plotting (αhν) 2 against photon energy (hν) gives a straight line with intercept equal to the optical energy band gap for direct transitions as shown in Fig. 12. The perovskite $ZnTiO_3$ has indirect energy gap (Egind) with the value 32.44 to 2 eV This means that the sintering temperature plays an important rule in the change optical energy gap for the investigated samples, The extinction coefficients K for the prepared samples were evaluated using the relation:

$$K=\alpha\lambda/4\pi$$

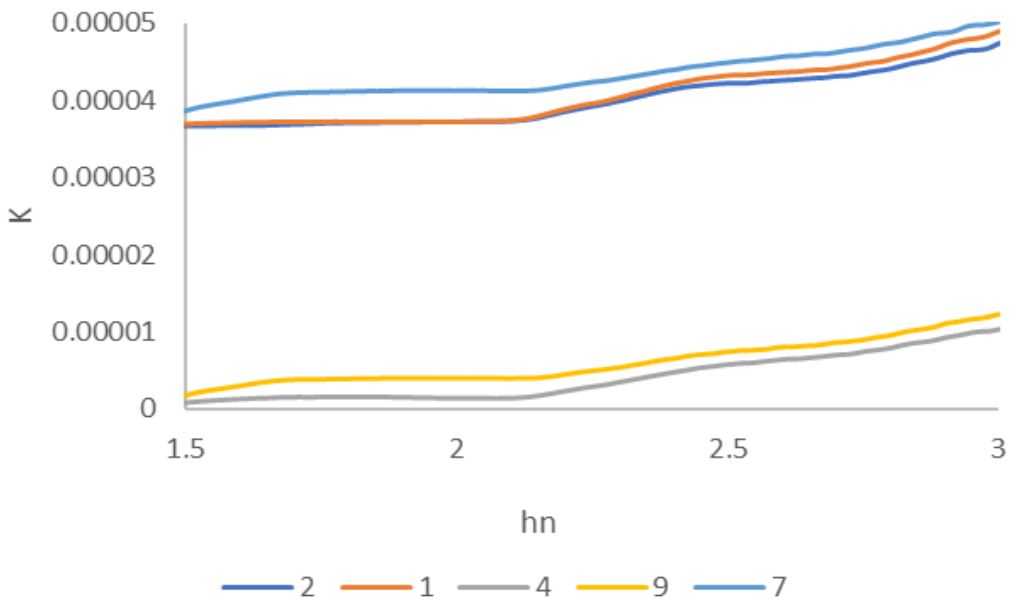

Fig 13:-Presented the relation between extinction coefficients of ZnTiO3 and the photon energy. It can be noticed that the extinction coefficient of the ZnTiO3 samples has the same behavior absorption.

Table 2:-Table (3.2) Effect of calcination temperature on the optical parameters

Samples	Optical gap energy	Urbakh energy
500^0C	2.44ev	0.775 e.v
600^0C	2.35 ev	0.78 e.v
700^0C	2.16 ev	0.783 e.v
900^0C	2 ev	0.9898 e.v

Conclusion:-

The formation of crystalline phase of synthesized product was confirmed by XRD measurements.

The results indicated a strong dependence of the microstructural, morphological, optical and on Zn:Ti molar ratios which bear a direct influence on the photocatalytic performance of the composites

UV-Vis spectra showed that all samples exhibited good absorption towards UV region. The calculated energy band gaps of $ZnTiO_3$ are 2.92 eV which is slightly smaller compared to bulk ZnO and TiO_2 . The tuning energy band gaps of ZnO-TiO_2 composite samples is a good indicator for use in catalytic activities.

The optical properties of the nano perovskite $ZnTiO_3$ revealed bandgap energies (Eg) that varied with the temperature attaining a minimum value of 2. eV. It was observed that the reported Eg was lower compared to the bandgap energies individual semiconductor oxides and was well-matched with the**Lawrence Kioko Munguti and F. B. Dejene (2021Asiah Mohd Nor , Mohd Firdaus Malek and R. MohamedomeMaterials Science ForumMaterials Science Forum Vol. 1055**

References:-

1-Y.M. Meor, E.M. Mahdi, P. Wilfred, M. Masliana**Photocatalytic active nanorutile TiO_2: synthesis characterization and photocatalysis tests**
J Nano Res, 26 (2013), p. 17
CrossRefGoogle Scholar
2-H.M. Yadav, S.C. Jung, J.S. Kim**Visible Light photocatalytic performance of in situ synthesized graphite-SiO_2–TiO_2 composite towards degradation of benzene gas**
J NanosciNanotechnol, 18 (3) (2018), pp. 2032-2036

3-Synthesis, characterization and investigation of photocatalytic activity of nano-Author links open overlay panelNatrahShafiqahRosli[abc]CheAzurahanimCheAbdullah[ab]RoshasnorlyzaHazan**Results in Physics**Volume 11, December 2018, Pages 72-78

4-Comparison of photocatalytic reaction of commercial P25 and synthetic TiO2-AgCl nanoparticles
W. Sangchaya , L. Sikonga,b*, K. Kooptarnonda,b
a Department of Mining and Materials Engineering, Faculty of Engineering, Prince of Songkla University (PSU), Hat Yai, Thailand b NANOTEC Center of Excellence at Prince of Songkla University, Thailand Elsevier use only: Received 30 September 2011; Revised 10 November 2011; Accepted 25 November 2011.
Procedia Engineering 32 (2012) 590 – 596

5-Aghababaei, N. (2016). Synthesis and characterization of Mg / TiO 2 nano-composites for electrical resistivity. 48(D), 21–24.

6-Ahmed, S., & Hejjawi, H. (2013). TiO 2 and ZnO photocatalysts for degradation of widespread pharmaceutical wastes : Effect of particle size and support

7-Bandara, J., Hadapangoda, C. C., & Jayasekera, W. G. (2004). TiO2/MgO composite photocatalyst: The role of MgO in photoinduced charge carrier separation. Applied Catalysis B: Environmental, 50(2), 83–88. https://doi.org/10.1016/j.apcatb.2003.12.021

8-Bayal, N., & Jeevanandam, P. (2014). Synthesis of TiO2-MgO mixed metal oxide nanoparticles via a sol-gel method and studies on their optical properties. Ceramics International, 40(10), 15463–15477. https://doi.org/10.1016/j.ceramint.2014.06.122

9-Bello Lamo, M. P., Williams, P., Reece, P., Lumpkin, G. R., & Sheppard, L. R. (2014). Study of gamma irradiation effect on commercial TiO2 photocatalyst. Applied Radiation and Isotopes, 89, 25–29. https://doi.org/10.1016/j.apradiso.2014.02.001

10-Ch, A., K, V. R., & Ch, S. C. (2015). Nanomedicine & Nanotechnology Synthesis and Characterization of MgO / TiO 2 Nanocomposites. 6(6), 2–6. https://doi.org/10.4172/2157-7439.1000329

11-Dahl, M., Liu, Y., & Yin, Y. (2014). Composite titanium dioxide nanomaterials. Chemical Reviews, 114(19), 9853–9889. https://doi.org/10.1021/cr400634p

12-Das, A., Patra, M., Wary, R. R., Gupta, P., & Nair, R. G. (2018). Photocatalytic performance analysis of Degussa P25 under various laboratory conditions. IOP Conference Series: Materials Science and Engineering, 377(1). https://doi.org/10.1088/1757-899X/377/1/012101

13-El-sayed, S. M., Amer, M. A., Meaz, T. M., Deghiedy, N. M., & El-shershaby, H. A. (2017). Effect of Radiation on the Structure and Optical Absorption Properties for Binary Oxide System E ff ect of radiation on the structure and optical absorption properties for binary oxide system. Measurement, 112(August), 99–104. https://doi.org/10.1016/j.measurement.2017.08.028

14-Grocholl, L. (2005). Solid-state synthesis. Nature Nanotechnology, 13(1), 4–4. https://doi.org/10.1038/s41565-017-0056-0

15-Gutierrez, J., Tercjak, A., Martin, L., & Mondragon, I. (2011). Electrical properties of TiO2/SEO nanocomposites: From macro to nano. Electrochimica Acta, 56(16), 5582–5586. https://doi.org/10.1016/j.electacta.2011.03.135

16-Hanaor, D. A. H., & Sorrell, C. C. (2011). Review of the anatase to rutile phase transformation. Journal of Materials Science, 46(4), 855–874. https://doi.org/10.1007/s10853-010-5113-0

17-Jung, H. S., Lee, J. K., Nastasi, M., Lee, S. W., Kim, J. Y., Park, J. S., … Shin, H. (2005). Preparation of nanoporous MgO-coated TiO 2 nanoparticles and their application to the electrode of dye-sensitized solar cells. Langmuir, 21(23), 10332–10335. https://doi.org/10.1021/la051807d

18-Landmann, M., Rauls, E., & Schmidt, W. G. (2012). The electronic structure and optical response of rutile, anatase and brookite TiO 2. Journal of Physics Condensed Matter, 24(19). https://doi.org/10.1088/0953-8984/24/19/195503

19-Lisnycha, T. V., Kirillov, S. A., Potapenko, A. V., Terikovska, T. E., Kosilov, V. V., & Vyshnevskiy, O. A. (2016). Hydrothermal synthesis of anatase nanoleaves and size dependence of anatase–rutile transformation upon heating. International Nano Letters, 6(2), 111–117. https://doi.org/10.1007/s40089-015-0174-3

20-Marcos Fernández-Garcia, J. A. R. (2007). Metal Oxide Nanoparticles. Encyclopedia of Inorganic Chemistry, (October). https://doi.org/10.1002/0470862106.ia377

21. Pankove I. J., Optical Process in Semiconductors, Prentice-Hall, Inc., (1971).

22-Mbarki, R., Hamzaoui, A. H., & Mnif, A. (2015). Dielectric properties and electrical conductivity of MgO synthesized by chemical precipitation and sol-gel method. EPJ Applied Physics, 69(1). https://doi.org/10.1051/epjap/2014130287

23-McMillan, P. F., Gryko, J., Bull, C., Arledge, R., Kenyon, A. J., & Cressey, B. A. (2005). Amorphous and

nanocrystalline luminescent Si and Ge obtained via a solid-state chemical metathesis synthesis route. Journal of Solid State Chemistry, 178(3), 937–949. https://doi.org/10.1016/j.jssc.2004.12.040

24-Meng, F., Dehouche, Z., Nutasarin, A., & Fern, G. R. (2018). Effective MgO-doped TiO2 nanoaerogel coating for crystalline silicon solar cells improvement. International Journal of Energy Research, 42(12), 3915–3927. https://doi.org/10.1002/er.4128

25-Moghaddam, H. M., & Nasirian, S. (2012). Dependence of activation energy and lattice strain on TiO 2 nanoparticles? . Nanoscience Methods, 1(1), 201–212. https://doi.org/10.1080/17458080.2011.620023

26-Obeid, B. G., Hameed, A. S., & Alaaraji, H. H. (2017). Structural and optical properties of TiO 2:MgOo thin films preparing at 373K. Digest Journal of Nanomaterials and Biostructures, 12(4), 1239–1246.

27-Piyush, S. (2010). Studies on Mixed Oxide Functional Ceramics Ph . D . Thesis Submitted to Saurashtra University , Rajkot , India By Piyush S . Solanki Research Guide Prof . D . G . Kuberkar April 2010.

28-Sabree, I. K. (2018). THE EFFECT OF TiO2 AS ADDITIVES ON PROPERTIES OF COMPOSITE MgO FOR BONE REPAIR. The Iraqi Journal for Mechanical and Materials Engineering, 18(2), 229–238. https://doi.org/10.32852/iqjfmme.vol18.iss2.88

29-Sathish Kumar, K., Rohit Narayanan, K. R., Siddarth, S., Pavan Kumar, R., Badri Narayan, R., Goutham, R., & Samynaathan, V. (2018). Synthesis of MgO/TiO2 Nanocomposite and Its Application in Photocatalytic Dye Degradation. International Journal of Chemical Reactor Engineering, 16(8), 1–14. https://doi.org/10.1515/ijcre-2017-0136

30-Sharma, I., Ambika, & Barman, P. B. (2008). Electrical properties of magnesium oxide thin films. Optoelectronics and Advanced Materials, Rapid Communications, 2(10), 640–642.

31-Shivaraju, H. P., Midhun, G., Anil Kumar, K. M., Pallavi, S., Pallavi, N., & Behzad, S. (2017). Degradation of selected industrial dyes using Mg-doped TiO2 polyscales under natural sun light as an alternative driving energy. Applied Water Science, 7(7), 3937–3948. https://doi.org/10.1007/s13201-017-0546-0

32-Shrestha, K. M., Sorensen, C. M., & Klabunde, K. J. (2013). MgO-TiO2 mixed oxide nanoparticles: Comparison of flame synthesis versus aerogel method; Characterization, and photocatalytic activities. Journal of Materials Research, 28(3), 431–439. https://doi.org/10.1557/jmr.2012.288

33-Skocaj, M., Filipic, M., Petkovic, J., & Novak, S. (2011). Titanium dioxide in our everyday life; Is it safe? Radiology and Oncology, 45(4), 227–247. https://doi.org/10.2478/v10019-011-0037-0

34-Taguchi, T., Zhang, X. T., Sutanto, I., Tokuhiro, K. I., Rao, T. N., Watanabe, H., … Fujishima, A. (2003). Improving the performance of solid-state dye-sensitized solar cell using MgO-coated TiO2 nanoporous film. Chemical Communications, 3(19), 2480–2481. https://doi.org/10.1039/b306118c.